CMS Physics Analysis Summary

Contact: cms-pag-conveners-exotica@cern.ch 2016/03/26

Search for high-mass resonances in $Z\gamma \to e^+e^-\gamma / \mu^+\mu^-\gamma$ final states in proton-proton collisions at $\sqrt{s} = 13$ TeV

The CMS Collaboration

Abstract

A search for a heavy resonance decaying to $Z\gamma$, with the Z boson further decaying to pairs of electrons or muons is presented. The search makes use of 13 TeV proton-proton collision data collected by the CMS experiment at the LHC, corresponding to an integrated luminosity of 2.7 fb^{-1}. The analysis extracts the background directly from data, through an unbinned likelihood fit. No signifcant excess over the background-only hypothesis is observed, therefore limits at 95% confidence level are set on the production cross section of particles with a mass between 350 GeV and 2 TeV, with two different assumptions on the resonance width.

1 Introduction

The discovery of a Higgs boson at 125 GeV [1, 2], while generally seen as the completion of the Standard Model (SM) of particle physics, can also be viewed as a first piece of evidence of a larger and much sought-after theory to which the SM would only be a low energy approximation. A modest excess of data over the expected background in the diphoton spectrum around the invariant mass of 750 GeV observed both by the ATLAS [3] and the CMS [4] collaborations, if confirmed, could be a second piece to this picture. Adding a scalar (or similarly a pseudoscalar) with mass m_A to the Standard Model and assuming no extra tree-level decays other than an effective coupling to gluons and to SM gauge bosons, implies [5] that there could be large contributions to the $Z\gamma$ decay, such that it could be visible at 13 TeV.

This note describes the results of a search for heavy resonances with a mass between 350 GeV and 2 TeV decaying to $Z\gamma$, with further decay $Z \to \ell^+\ell^-$, with $\ell = e, \mu$. The search is based on 13 TeV proton-proton collision data collected by the CMS experiment in 2015, corresponding to 2.7 fb^{-1} of integrated luminosity. The search strategy measures the non-resonant background directly on data, and looks for localized excesses, similarly to what is done in [4]. Searches for resonances decaying to $Z\gamma$ have also been performed at $\sqrt{s} = 8$ TeV by both CMS [6] and ATLAS [7].

2 CMS Detector and Object Reconstruction

A detailed description of the CMS detector can be found elsewhere [8]. The central feature of the CMS apparatus is a superconducting solenoid, 13 m in length and 6 m in diameter, which provides an axial magnetic field of 3.8 T. Within the field volume there are several particle detection systems. Charged-particle trajectories are measured by silicon pixel and strip trackers, covering $0 < \phi < 2\pi$ in azimuth and $|\eta| < 2.5$ in pseudorapidity, where η is defined as $\eta = \ln[\tan(\theta/2)]$ and θ is the polar angle of the trajectory of the particle with respect to the counterclockwise proton beam direction. A lead tungstate crystal electromagnetic calorimeter (ECAL) is partitioned into a barrel region with $|\eta| < 1.48$ and two endcaps that extend up to $|\eta| = 3$. A brass and scintillator hadron calorimeter surrounds the ECAL volume and covers the region $|\eta| < 3$. Iron forward calorimeters with quartz fibers, read out by photomultipliers, extend the calorimeter coverage up to $|\eta| = 5$. They provide measurements of the energy of photons, electrons, and hadronic jets. A lead and silicon-strip preshower detector is located in front of the endcap electromagnetic calorimeter. Muons are identified and measured in gas-ionization detectors embedded in the steel return-yoke outside the solenoid. The detector is nearly hermetic, allowing energy balance measurements in the plane transverse to the beam direction. A two-tier trigger system selects proton-proton collision events of interest for use in physics analysis.

Event reconstruction is based on the particle-flow algorithm [9, 10], which combines information from the tracker, calorimeter, and muon systems to reconstruct and identify charged and neutral hadrons, photons, muons and electrons. To select collision events we require at least one reconstructed vertex. If more than one vertex is reconstructed, we designate as the primary vertex the one for which the sum p_{T}^2 of the associated particle-flow candidates is largest.

Photon candidates are reconstructed from the energy deposits in the ECAL, grouping them into superclusters. The superclustering algorithms achieve an almost complete collection of the energy of photons (and electrons) that convert into electron-positron pairs in the material in front of the ECAL. In the barrel region, superclusters are formed from five-crystal-wide strips in η, centered on the locally most energetic crystal (seed), and have a variable exten-

sion in ϕ. In the endcaps, where the crystals are arranged according to an x-y rather than an $\eta - \phi$ geometry, matrices of 5×5 crystals (which may partially overlap) around the most energetic crystals are merged if they lie within a narrow ϕ strip. The photon candidates are collected within the ECAL fiducial region $|\eta| < 2.5$, excluding the barrel-endcap transition region $1.44 < |\eta| < 1.57$, and are selected by making simple rectangular requirements on the cluster shower shape and on the ratio between the reconstructed energy and the deposit of energy in the hadronic calorimeter right behind the ECAL seed. Isolation requirements are applied to photon candidates by requiring the total scalar sum of the transverse momenta of charged tracks within $\Delta R = \sqrt{\Delta\eta^2 + \Delta\phi^2} = 0.3$ to be less than 2.5 GeV, where $\Delta\eta$ and $\Delta\phi$ are, respectively, the difference in pseudorapidity and azimuth between the photon and the given track. Details on photon reconstruction and identification are found in [11].

Electron candidates [12] are reconstructed as a cluster of energy deposits in the electromagnetic calorimeter matched to signals in the silicon tracker. We identify electrons by loose requirements on the shape of these energy deposits, on the ratio of energy in associated hadron and electromagnetic calorimeter cells, on the geometric matching between the energy deposits and the associated track, and on consistency between the energy reconstructed from calorimeter deposits and the momentum measured in the tracker. We additionally require that the associated track is consistent with originating from the primary vertex.

Muon candidates [13] are reconstructed from tracks found in the muon system, associated to tracks in the silicon tracking detectors. The associated silicon track is required to be consistent with originating from the primary vertex. Muon identification criteria are based on the quality of the track fit and the number of associated hits in the different tracking detectors.

Lepton isolation is determined using a cone size dependent on the lepton p_{T} according to the equation:

$$\Delta R = \begin{cases} 0.2, & p_{\mathrm{T}} < 50 \text{ GeV} \\ \frac{10 \text{ GeV}}{p_{\mathrm{T}}}, & 50 < p_{\mathrm{T}} < 200 \text{ GeV} \\ 0.05, & p_{\mathrm{T}} > 200 \text{ GeV}. \end{cases} \tag{1}$$

The isolation sum is calculated using reconstructed neutral and charged particle-flow candidates and is corrected for the effects of pile-up. Electron (muon) candidates are required to have an isolation value less than 0.1 (0.2) of their transverse momentum. This ensures high lepton identification efficiency even for highly-boosted Z boson decays, where the two leptons are close to each other, as in the decay of heavy resonances.

3 Simulated Samples

Scalar resonances decaying to $Z\gamma$ are generated with PYTHIA [14, 15]. Several samples were generated with masses ranging from 350 GeV to 2 TeV, and for two resonance widths: a narrow resonance model, where the width is fixed to be equal to 0.014% of the scalar mass, and a wide model, with a 5.6% width.

Simulated background samples do not enter the analysis directly, as the background is obtained from a fit of the data, but have been used to assess the accuracy on background model, as described in Section 5. Standard model production of non-resonant $Z + \gamma$, which is expected to be the dominant background process, has been generated at next-to-leading-order accuracy with the MADGRAPH generator [16], interfaced with PYTHIA. Events in which a Z boson is produced in association with a jet, and the latter is mis-identified as a photon, constitute a sub-

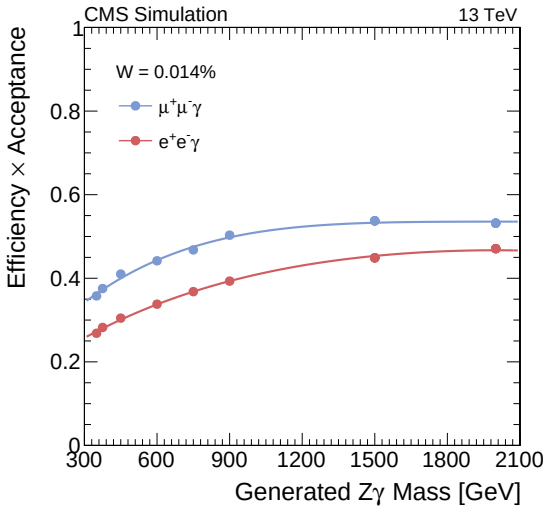

Figure 1: Expected signal efficiency after full selections, as a function of the generated resonance mass, for the $e^+e^-\gamma$ (red) and $\mu^+\mu^-\gamma$ (blue) channels in narrow-width signals.

dominant source of background, and have been generated at leading-order accuracy with the MADGRAPH generator, interfaced with PYTHIA.

4 Event Selection

Events are selected with exactly two opposite-sign electron or muons, and a photon. Events are required to have passed either a double-electron, double-muon, or single-muon trigger paths, with varying p_{T} thresholds. The trigger efficiency of this combination of trigger paths is above 95% (99%) for events in the search region of the $e^+e^-\gamma$ ($\mu^+\mu^-\gamma$) channel. The leading and subleading leptons are required to have $p_{\mathrm{T}} > 25, 20$ GeV, respectively. The chosen transverse momentum thresholds ensure that trigger turn-on effects may be neglected. Finally, the dilepton system is required to have an invariant mass between 50 and 130 GeV.

The photon is required to have $p_{\mathrm{T}} > 40$ GeV to have a distance $\Delta R > 0.4$ from each of the two leptons, to minimize the effect of lepton final state radiation. Finally, the photon transverse momentum has to be greater than $p_{\mathrm{T}} > \frac{40}{150} \cdot m_{Z\gamma}$, where $m_{Z\gamma}$ is the invariant mass of the dilepton+photon system. This requirement is found to have an efficiency of about 50% on the backgrounds, while retaining more than 90% of the signal.

Figure 1 shows the expected narrow signal efficiency after full selections, as a function of the generated resonance mass, for the $e^+e^-\gamma$ (red) and $\mu^+\mu^-\gamma$ (blue) channels. The lines represent the results of polynomial fits to the markers, and as can be seen the muon (electron) channel efficiency increases from about 35% (25%) at $m_A = 350$ GeV, to about 55% (45%) at $m_A = 2$ TeV. Studies of the simulation show that about 90% of the the background is composed of SM production of $Z\gamma$, while the remaining 10% is due to the production of a Z boson in association with a jet with high electromagnetic energy fraction, which simulates a photon.

The search variable $m_{Z\gamma}$ is scanned in the $m_{Z\gamma} > 200$ GeV region, separately in the $e^+e^-\gamma$ and $\mu^+\mu^-\gamma$ channels. The analysis searches for localized excesses consistent with resonant $Z\gamma$ production, for particles with masses in the $350 - 2000$ GeV range. The analysis has been performed following a blinding policy, which means that the strategy was defined on the simulation before looking at the data in the search region.

5 Background Modelling

The non-resonant background $m_{Z\gamma}$ spectrum can be described by a parametric function of $m_{Z\gamma}$:

$$f(m_{Z\gamma}) = m_{Z\gamma}^{a+b\log m_{Z\gamma}}. \quad (2)$$

The parametric coefficients are obtained from a fit to the data events, and considered as unconstrained nuisance parameters in the hypothesis test, allowing to build a data-driven description of the shape.

The accuracy on the background estimation is assessed using Monte Carlo simulations and it is quantified by studying the difference between the true and predicted number of background events in different $m_{Z\gamma}$ windows in the search region. The mass spectrum predicted by the simulation is fitted with a number of test functions $g_i(m_{Z\gamma})$, and the result of the fit $\hat{g}_i(m_{Z\gamma})$ is used as truth model from which a large number of pseudo-experiments is drawn. The total number of events in each pseudo-experiment is taken from a Poisson distribution where the mean is fixed to be equal to the observation in data. Each pseudo-experiment is then fitted with the reference function $f(m_{Z\gamma})$, and for each mass window, the distribution of the pull variable, defined as the difference between the true ($\hat{g}_i$) and predicted (f) number of events divided by the estimated statistical uncertainty, is constructed. The absolute value of the median of this distribution shall be below 0.5 in the full search region. This criterion is equivalent to requiring that the uncertainty on the mean background yield, which in the statistical regime of this search is subdominant compared to the purely Poissonian term, is modelled with an accuracy better than 10%. In order to achieve this, the background uncertainty is inflated by a small term, which amounts to about 0.005 events/GeV at $m_{Z\gamma} = 600$ GeV, and smoothly falls to about 0.0005 events/GeV around $m_{Z\gamma} = 2$ TeV. Additional uncertainty, other than the statistical component relative to the fitting, are negligible for the $200 < m_{Z\gamma} < 600$ GeV region.

6 Signal Modelling

The signal distribution in $m_{Z\gamma}$ is obtained from the Monte Carlo simulation. The $m_{Z\gamma}$ distribution of simulated signal events that pass the full selection criteria is parameterized by a function with a Gaussian core and two power-law tails, an extended form of the Crystal Ball function [17].

The best-fit values of the six parameters of this function are measured on the simulated samples at each mass point, separately for the electron and muon channels, and then interpolated through linear fits to generic $m_{Z\gamma}$ values in order to have a smoothly-varying signal shape parametrization. It is found that for the electron channel the $m_{Z\gamma}$ resolution, defined from the gaussian core as σ/μ, is of about 1% across the considered mass spectrum, whereas for muons it worsens linearly with increasing resonance mass, from 1.4% at 350 GeV to 3% at 2 TeV.

7 Systematic Uncertainties on Signal

Systematic uncertainties on signal yields are computed on the simulated signal samples:

- **luminosity:** the uncertainty on the CMS integrated luminosity is based on pixel cluster counting from the silicon pixel detector [18] and amounts to 2.7%;
- **parton distribution functions:** we estimated a 1% uncertainty on the signal efficiency that takes into account the variation in the kinematic acceptance of the analysis coming from the use of alternative PDF sets;

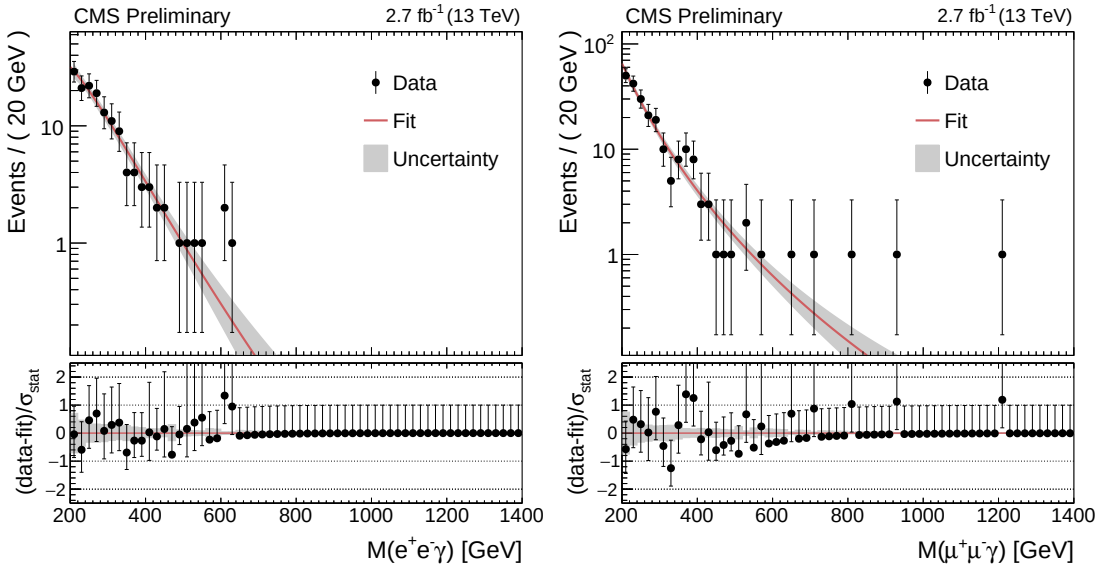

Figure 2: Fits of the $m_{Z\gamma}$ distribution in the data, for the $e^+e^-\gamma$ channel (left) and the $\mu^+\mu^-\gamma$ channel (right). Data are shown as black markers, in bins of 20 GeV, and the fitted function is represented by a red line, with the 68% uncertainty band as gray shade.

- **trigger:** the uncertainty due to trigger efficiency differences in data and in the simulation is estimated with dedicated studies with leptons on the Z peak and amounts to 2% (3%) for the muon (electron) channel;
- **lepton efficiency:** the systematic uncertainty on differences between data and simulation in lepton identification efficiency has been evaluated with $Z \to ee/\mu\mu$ events and amounts to 5%, both in the $e^+e^-\gamma$ and in the $\mu^+\mu^-\gamma$ channel;
- **photon efficiency:** the systematic uncertainty on differences between data and simulation in photon identification efficiency has been evaluated with $Z \to ee$ events in which the electrons are reconstructed as photons, and it amounts to 5%;
- **electron and photon energy scale:** the electron and photon energy scale is measured with 1% precision. This takes into account the knowledge of the energy scale at the Z peak and of its extrapolation to higher energies. This translates into a 1% (0.5%) correlated uncertainty on the $m_{Z\gamma}$ scale for the $e^+e^-\gamma$ ($\mu^+\mu^-\gamma$) channel;
- **muon momentum scale:** the muon momentum scale is measured with $\approx 1\%$ precision up to $p_{\mathrm{T}} = 200$ GeV. For muons with higher momentum, the uncertainty scales with the track curvature $1/p_{\mathrm{T}}$ as 10%/TeV (20%/TeV) for muons which are reconstructed in the barrel (endcaps); the effect on the mass scale increases with the signal mass, from about 0.5% at $m_A = 350$ GeV to about 5% at $m_A = 2$ TeV.

8 Results

Figure 2 shows the results of the fits of the $m_{Z\gamma}$ distribution for the $e^+e^-\gamma$ channel (left) and the $\mu^+\mu^-\gamma$ channel (right).

We set upper limits on the production cross section of heavy scalar resonances using the modified frequentist method, commonly known as CLs following the prescription in [19]. Asymptotic formulae [20] are used in the calculation.

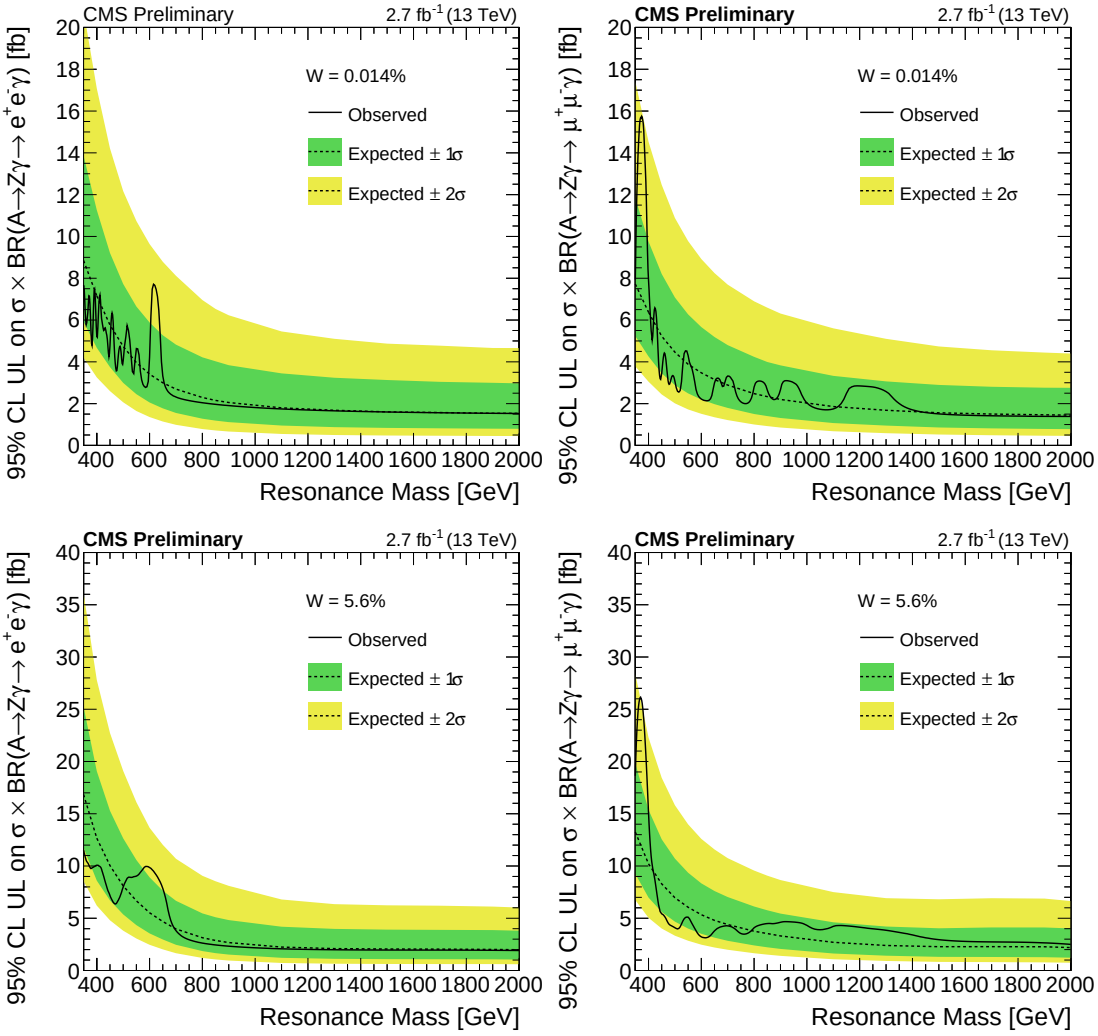

Figure 3: Observed (solid) and expected (dashed) 95% C.L. exclusion limits on $\sigma(A \to Z\gamma \to \ell^+\ell^-\gamma)$, as a function of signal mass, together with the 68% and 95% ranges of expectation in the background-only hypothesis, separately for the $e^+e^-\gamma$ (left) and $\mu^+\mu^-\gamma$ (right) channels. The top row shows limits on a narrow width signal, the bottom row on a wide width signal.

Figure 3 shows the expected 95%-confidence-level upper limits on $\sigma(A \to Z\gamma \to \ell^+\ell^-\gamma)$, as a function of the resonance mass, for the $e^+e^-\gamma$ channel (left) and the $\mu^+\mu^-\gamma$ channel (right) separately, for narrow (top) and wide (bottom) signal models. The expected limit for the background-only hypothesis is represented by a dashed black line, and its 68% and 95% ranges of expectation are shown with green and yellow bands, respectively. The observed limit is represented by a solid black line. The limits on $\sigma(A \to Z\gamma)$, obtained by combining the two search channels, are shown in Fig. 4, for the narrow (left) and wide (right) signal models.

An alternative cross-check cut-based analysis has been performed as well. This analysis uses a multivariate approach for electron and photon identification [11]. The leading electron (muon) is required to have $p_{\mathrm{T}} > 25$ (20) GeV, whereas the sub-leading electron (muon) is required to have $p_{\mathrm{T}} > 20$ (15) GeV. The dilepton invariant mass is required to be in the $60 - 120$ GeV range. The photon is required to have $p_{\mathrm{T}} > 140$ GeV, and to be reconstructed in the barrel ($|\eta| < 1.44$).

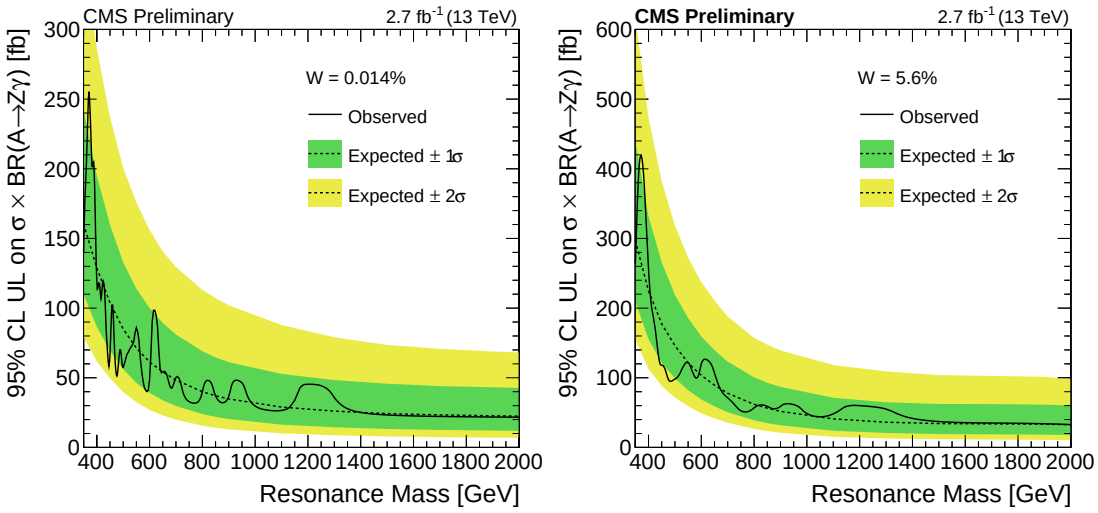

Figure 4: Observed (solid) and expected (dashed) 95% C.L. exclusion limits on $\sigma(A \to Z\gamma)$ as a function of signal mass, together with the 68% (green) and 95% (yellow) ranges of expectation in the background-only hypothesis. The range $350 < m_{Z\gamma} < 2000$ GeV is shown, for narrow width (left) and wide width signals (right).

The irreducible background is estimated from the simulation, whereas, the reducible background of jets mis-identified as photons is estimated from data. The search is performed in an optimized window around the mass hypothesis, with a width equal to 3% of m_A for low masses and up to to 6% of m_A for high masses, where the background becomes negligible. The cut-based analysis confirms the limits obtained by the fit based analysis in the high mass region, while in the low mass region the fit-based analysis has better limits, as expected since the cut based analysis does not use the shape information of the signal.

9 Conclusions

A search for heavy resonances with mass between 350 GeV and 2 TeV decaying to $Z\gamma$, with further decay $Z \to \ell^+\ell^-$, with $\ell = e, \mu$, has been presented. The search makes use of 13 TeV proton-proton collision data collected by the CMS experiment at the LHC, corresponding to an integrated luminosity of 2.7 fb^{-1}. The search strategy measures the non-resonant background directly on data, and looks for localized excesses. No significant excess over the Standard Model expectation is found, and limits at 95% confidence level are set on the production cross section of resonances for masses between 350 GeV and 2 TeV for two different hypothetical signal widths.

References

[1] S. Chatrchyan et al., "Observation of a new boson at a mass of 125 GeV with the CMS experiment at the LHC", *Physics Letters B* **716** (2012) 30 – 61, doi:10.1016/j.physletb.2012.08.021.

[2] G. Aad et al., "Observation of a new particle in the search for the Standard Model Higgs boson with the ATLAS detector at the LHC", *Physics Letters B* **716** (2012) 1 – 29, doi:10.1016/j.physletb.2012.08.020.

[3] ATLAS Collaboration, "Search for resonances decaying to photon pairs in 3.2 fb^{-1} of pp collisions at $\sqrt{s}$ = 13 TeV with the ATLAS detector", ATLAS-CONF 2015/081, 2015.

[4] CMS Collaboration, "Search for new physics in high mass diphoton events in proton-proton collisions at $\sqrt{s} = 13$ TeV", Technical Report CMS-PAS-EXO-15-004, CERN, 2015.

[5] D. Buttazzo, A. Greljo, and D. Marzocca, "Knocking on New Physics' door with a Scalar Resonance", technical report, 2015. arXiv:1512.04929.

[6] CMS Collaboration, "Search for scalar resonances in the 200-1200 GeV mass range decaying into a Z and a photon in pp collisions at $\sqrt{s} = 8$ TeV", Technical Report CMS-PAS-HIG-16-014, CERN, 2016.

[7] G. Aad et al., "Search for new resonances in $W\gamma$ and $Z\gamma$ final states in pp collisions at with the ATLAS detector", *Physics Letters B* **738** (2014) 428 – 447, doi:http://dx.doi.org/10.1016/j.physletb.2014.10.002.

[8] CMS Collaboration, "The CMS experiment at the CERN LHC", *JINST* **3** (2008) S08004, doi:10.1088/1748-0221/3/08/S08004.

[9] CMS Collaboration, "Particle-Flow Event Reconstruction in CMS and Performance for Jets, Taus, and MET", Technical Report CMS-PAS-PFT-09-001, CERN, 2009.

[10] CMS Collaboration, "Commissioning of the Particle-flow Event Reconstruction with the first LHC collisions recorded in the CMS detector", Technical Report CMS-PAS-PFT-10-001, CERN, 2010.

[11] CMS Collaboration, "Performance of photon reconstruction and identification with the CMS detector in proton-proton collisions at $\sqrt{s} = 8$ TeV", *JINST* **10** (2015) P08010, doi:10.1088/1748-0221/10/08/P08010.

[12] CMS Collaboration, "Electron reconstruction and identification at sqrt(s) = 7 TeV", Technical Report CMS-PAS-EGM-10-004, CERN, 2010.

[13] CMS Collaboration, "Performance of CMS muon reconstruction in pp collision events at $\sqrt{s} = 7$ TeV", *JINST* **7** (2012) P10002, doi:10.1088/1748-0221/7/10/P10002.

[14] T. Sjöstrand, S. Mrenna, and P. Skands, "PYTHIA 6.4 physics and manual", *JHEP* **05** (2006) 026, doi:10.1088/1126-6708/2006/05/026.

[15] T. Sjöstrand et al., "An Introduction to PYTHIA 8.2", *Comput. Phys. Commun.* **191** (2015) 159–177, doi:10.1016/j.cpc.2015.01.024.

[16] J. Alwall et al., "The automated computation of tree-level and next-to-leading order differential cross sections, and their matching to parton shower simulations", *JHEP* (2014) 079, doi:10.1007/JHEP07(2014)079.

[17] M. Oreglia, "A Study of the Reactions $\psi' \to \gamma\gamma\psi$". PhD thesis, SLAC, 1980.

[18] CMS Collaboration, "CMS Luminosity Measurement for the 2015 Data Taking Period", Technical Report CMS-PAS-LUM-15-001, CERN, 2016.

[19] A. Read, "Modified frequentist analysis of search results (the CL_s method)", Technical Report CERN-OPEN-2000-005, CERN, 2000.

[20] G. Cowan, K. Cranmer, E. Gross, and O. Vitells, "Asymptotic formulae for likelihood-based tests of new physics", *Eur.Phys.J.* **C71** (2011) 1554, doi:10.1140/epjc/s10052-011-1554-0, 10.1140/epjc/s10052-013-2501-z.